Ansari-Rad; M., Athanasopoulos, S. (2018).Theoretical study of equilibrium and nonequilibrium exciton dynamics in disordered semiconductors. *Physical Review B*, 98(8).

DOI: https://doi.org/10.1103/PhysRevB.98.085204

Theoretical study of equilibrium and nonequilibrium exciton dynamics in disordered semiconductors

Mehdi Ansari-Rad*
Department of Physics, Shahrood University of Technology, Shahrood 3619995161, Iran

Stavros Athanasopoulos†
Departamento de Física, Universidad Carlos III de Madrid, Avenida Universidad 30, Leganés 28911, Madrid, Spain

(Received 16 May 2018; published xxxxxx)

We develop a temperature-dependent theory for singlet exciton hopping transport in disordered semiconductors. It draws on the transport level concept within a Förster transfer model and bridges the gap in describing the transition from equilibrium to nonequilibrium time-dependent spectral diffusion. We test the validity range of the developed model using kinetic Monte Carlo simulations and find agreement over a broad range of temperatures. It reproduces the scaling of the diffusion length and spectral shift with the dimensionless disorder parameter and describes in a unified manner the transition from equilibrium to nonequilibrium transport regime. We find that the diffusion length in the nonequilibrium regime does not scale with the the third power of the Förster radius. The developed theory provides a powerful tool for interpreting time-resolved and steady state spectroscopy experiments in a variety of disordered materials, including organic semiconductors and colloidal quantum dots.

DOI: 10.1103/PhysRevB.00.005200

I. INTRODUCTION

The phenomenon of exciton diffusion is found to play a role in a remarkably wide range of physical systems, including disordered organic semiconductors [1,2], nanocrystalline quantum dots [3–6], semiconducting carbon nanotubes [7–10], and photosynthetic biological systems [11]. Moreover, there is a growing interest in describing electronic excitation energy transfer because exciton dynamics determines function in many technological applications. For example, in thin-film organic solar cells, exciton diffusion drives charge separation [12,13], in organic light emitting diodes it determines the brightness and color of the device [14], in scintillator detectors it controls the response function and yield [15], while in quantum communication systems it facilitates photon antibunching [16].

In disordered semiconductors that display weak intermolecular interactions, excitations created upon light absorption, carrier recombination, or annihilation processes are typically Frenkel excitons that are localized on single chromophore units (molecule, conjugated segment, quantum dot) and have a finite lifetime before relaxation to the ground electronic state occurs by radiative or nonradiative process. In the weak coupling regime, excitons transfer from one unit to the other with a Markovian incoherent hopping process and transport can be described as a simple diffusive motion [17]. However, chromophore units are not equivalent to each other as they can have different on-site excitation energies due to the different local environment, structure, or size as well as different excitonic couplings with neighbors. As a consequence, the energy landscape has a distribution that is often approximated by a Gaussian [18] and the standard deviation of the distribution defines the disorder parameter σ. Therefore, in the course of time, excitations sample the energetic landscape and on average relax to lower energy sites until they "settle down" to a steady state and equilibrium is achieved. However, because excitations have a finite lifetime τ, the relaxation process might be incomplete and, consequently, the exciton transport out of equilibrium [19]. It should be emphasized that this spectral relaxation process is different from the initial rapid vibronic relaxation [20]. Another consequence of the finite lifetime is that excitations have a limited spatial diffusion range, determined by the diffusion length L_D [19,21,22]. Spectroscopic techniques such as time-resolved and time-integrated photoluminescence spectroscopy can provide information on spectral diffusion [23–25] and a number of organic and inorganic systems have been studied over a range of temperatures [26–31].

A common misconception exists, that in practical device applications at room temperature, equilibrium transport prevails and the description of transport in terms of normal diffusion is sufficient. However, the distinction between equilibrium and nonequilibrium exciton transport is quite a subtle one and the transport regime is not uniquely defined only by temperature. Whilst significant progress has been made on understanding temperature dependent spectral relaxation and exciton diffusion, including experimental measurements [26–33] and computational models [19,21,33–44], currently there is no analytical theory that can describe the transition from equilibrium to nonequilibrium transport. In contrast, for *charges* it has been suggested that the transport problem can be modeled as a multiple-trapping process and it has been shown that a unique level in the energy distribution exists, the transport energy (TE), that plays the same role as the

*Electronic address: ansari.rad@shahroodut.ac.ir
†Electronic address: astavros@fis.uc3m.es

mobility edge in the multiple-trapping mechanism [45–47]. Note that in contrast to the long-range nature of the dipole-dipole interaction facilitating singlet exciton transport [48], charge transport in disordered semiconductors occurs via a short-range tunneling mechanism [49].

In this paper, we shall develop and test a theory that can treat the dynamics of exciton diffusion at both the equilibrium and nonequilibrium transport regime. In what follows, we develop a formalism based on the TE concept for the calculation of singlet exciton transport parameters, such as relaxation energy and diffusivity, including their temporal dependence. The validity of the TE level concept for Förster processes has been demonstrated by Baranovskii and Faber [50]. However, the TE level concept has not been applied yet to describe temperature and time dependent singlet exciton transport. In Sec. II, we repeat the main arguments and equations of Ref. [50] to enable the reader to follow theoretical consideration in Sec. III based on these equations. Section III includes the main results (Secs. III A, B, and E) along with a comparison of the theory to Monte Carlo simulations (Sec. III C), a discussion on the TE level concept for short vs long-range transfer and comparison with experiments (Sec. III D). Section IV summarizes the work and draws conclusions.

II. TRANSPORT ENERGY LEVEL FOR FÖRSTER TRANSFER

We consider thermally assisted Förster energy transfer between localized states described by the rate [19,50,51]

$$\nu(\varepsilon_d \to \varepsilon_a) = \frac{1}{\tau} S(R) \exp\left[-\frac{\Delta\varepsilon + |\Delta\varepsilon|}{2k_{\mathrm{B}}T}\right], \tag{1}$$

with

$$S(R) = \left(\frac{R_{\mathrm{F}}}{R}\right)^6, \tag{2}$$

where τ is the intrinsic exciton lifetime, R_{F} is the Förster radius, determined by the donor-acceptor spectral overlap, and $k_{\mathrm{B}}T$ is the thermal energy. $\Delta\varepsilon = \varepsilon_a - \varepsilon_d$ is the difference between the donor and acceptor energies and R is the corresponding distance.

We take into account a Gaussian distribution of energy states $g(\varepsilon) = N/\sqrt{2\pi\sigma^2}\exp(-\varepsilon^2/2\sigma^2)$, with N and σ the total density of states (DOS) and the width of the distribution, respectively. If the relaxation process is completed during the lifetime τ, excitons will occupy states around the equilibrium energy ε_∞ (see Fig. 1) at which the product $g(\varepsilon)f(\varepsilon,\varepsilon_F)$ maximizes [49]. Here, $f(\varepsilon,\varepsilon_F) = \{1+\exp[(\varepsilon-\varepsilon_F)/k_{\mathrm{B}}T]\}^{-1}$ is the Fermi distribution and ε_F is the Fermi level, determined by the number density n of the excitons as

$$n = \int_{-\infty}^{+\infty} g(\varepsilon) f(\varepsilon,\varepsilon_F)\mathrm{d}\varepsilon. \tag{3}$$

Note that at low densities, the equilibrium energy ε_∞ can be approximated by either $-\sigma^2/k_{\mathrm{B}}T$, at high temperatures [52], or by ε_F, at low temperatures; see Fig. 2(a).

Now, we examine the possibility of the existence of a TE level ε_{tr} in the energy distribution that can serve as the mobility edge in our exciton diffusion problem [50]. In the presence of such an energy level, excitons with $\varepsilon > \varepsilon_{tr}$, will, on average, move downward in the distribution, toward the TE level. On the other hand, upward jumps of excitons with $\varepsilon < \varepsilon_{tr}$ will be in the vicinity of ε_{tr}. If we express the mean jump distance as

$$R_{\varepsilon_{tr}} = \left[\frac{4\pi}{3}\int_{-\infty}^{\varepsilon_{tr}} g(\varepsilon) f'(\varepsilon,\varepsilon_F)\mathrm{d}\varepsilon\right]^{-1/3}, \tag{4}$$

we can obtain the following equation governing the position of the TE level for the Förster transport problem:

$$g(\varepsilon_{tr}) f'(\varepsilon_{tr},\varepsilon_F) = \frac{1}{2k_{\mathrm{B}}T}\int_{-\infty}^{\varepsilon_{tr}} g(\varepsilon) f'(\varepsilon,\varepsilon_F)\mathrm{d}\varepsilon, \tag{5}$$

where $f'(\varepsilon,\varepsilon_F) = 1 - f(\varepsilon,\varepsilon_F)$. We have used the approach of Ref. [46] to obtain the above equation, according to which one can find ε_{tr} by maximizing the upward transfer rate; see Appendix A for more details. We emphasize that the form of Eq. (5) directly follows from the inverse *sixth* power distance dependence of the dipole-dipole interaction. Equation (5) also shows that the position of ε_{tr} is independent of the characteristic length R_{F} and the density N, in contrast to the charge transport problem in which $\varepsilon_{tr} = \varepsilon_{tr}(\alpha, N)$. Interestingly, Eq. (5) does not acquire a solution for an exponential DOS. Again, this is in contrast to the charge transport problem, where for both Gaussian and exponential DOS one can find a TE level in the energy distribution. Charge transport in disordered semiconductors occurs via short-range transfer mechanism, with a rate similar to Eq. (1), but with $S(R) = \exp(-2R/\alpha)$, where α is the carrier localization length.

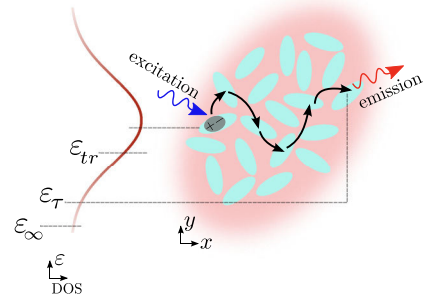

FIG. 1. Schematic illustration of interacting units in a disordered semiconductor, resulting in a Gaussian broadened excitonic DOS. Singlet exciton diffusion via Förster-type energy transfer process triggers energy relaxation toward the equilibrium energy ε_∞. Due to the finite lifetime, excitons may decay at a higher energy, ε_τ. ε_{tr} is the transport energy level.

Figure 2(a) illustrates ε_{tr} as a function of disorder normalized thermal energy. At high temperatures, ε_{tr} lies near the center of the energy distribution. At lower temperatures, ε_{tr} decreases to lower energies because by decreasing the temperature thermal activation to higher energies becomes less probable. We point out that a meaningful application of the TE level requires that the condition $\varepsilon_{tr} > \varepsilon_\infty$ [49] is satisfied. To test this condition, we plot a heat map of $\varepsilon_{tr} - \varepsilon_\infty$ as a function of $k_{\mathrm{B}}T/\sigma$ and excitation density in Fig. 2(b), which shows that this condition is fulfilled over a broad range of temperatures and exciton densities. Thus the concept of the TE can be used for Förster-type exciton transport. In what follows, we consider the weak excitation condition, with $n/N \ll 1$ and therefore $f' \approx 1$. More precisely, we use $\sigma = 0.065$ eV, $N = 1$ nm^{-3} and

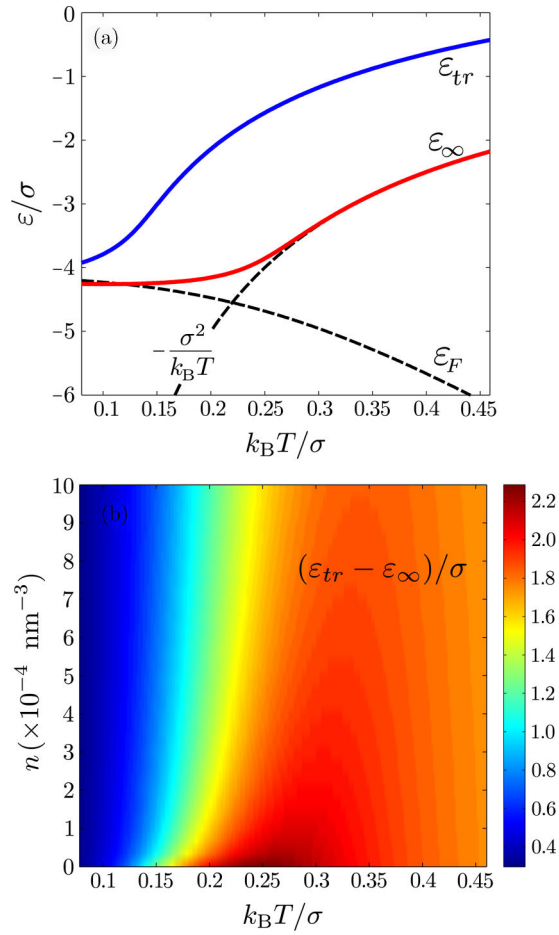

FIG. 2. (a) Transport energy level ε_{tr}, as a function of disorder normalized temperature. Data are obtained using Eq. (5) with $\sigma = 0.065$ eV, $N = 1\ \mathrm{nm}^{-3}$, and $n/N = 1.6 \times 10^{-5}$. ε_F is the Fermi level and ε_∞ is the thermal equilibrium energy, approaching $-\sigma^2/k_BT$ at high temperatures. (b) Heat map of $\varepsilon_{tr} - \varepsilon_\infty$ for a broad range of temperatures and exciton densities.

$n/N = 1.6 \times 10^{-5}$, corresponding to one exciton in a lattice of size $(40\ \mathrm{nm})^3$, as implemented in our kMC simulations. The same parameters were used in Fig. 2(a).

III. NONEQUILIBRIUM EXCITON DYNAMICS

A. Demarcation energy level and energy relaxation

Having outlined the concept of the TE level and the governing equations for singlet exciton transport [50], let us now turn our attention to the main problem, that is, the description of the relaxation dynamics. Excitons, generated randomly in the DOS, progressively thermalize into deeper energies. Notwithstanding their way to the deep energy levels, excitons need to be first activated to shallower energies, because the density of such levels is high in the energy distribution. Using the concept of the TE level we can say that these intermediate activations, necessary to approach thermal equilibrium, are most probable at the vicinity of the level ε_{tr}. As first introduced by Tiedje and Rose [53], we can define a demarcation energy $\varepsilon_m(t)$ in the system, such that during time t following the initial excitation, only the levels with $\varepsilon > \varepsilon_m(t)$ are likely to release their excitons to the TE level. Mathematically, this means that $t\nu(\varepsilon_m \to \varepsilon_{tr}) = \theta$, with θ being $\mathcal{O}(1)$. In a more explicit form,

$$t\frac{1}{\tau}\left(\frac{R_F}{R_{\varepsilon_{tr}}}\right)^6 \exp\left[-\frac{\varepsilon_{tr}-\varepsilon_m(t)}{k_BT}\right] = \theta. \tag{6}$$

From the above equation we find

$$\varepsilon_m(t) = \varepsilon_{tr} - k_BT \ln\left[\frac{t}{\theta\tau}\left(\frac{R_F}{R_{\varepsilon_{tr}}}\right)^6\right]. \tag{7}$$

On the other hand, if we consider the low density condition, we can obtain the following equation for the mean jump distance from Eqs. (4) and (5):

$$\frac{1}{R^3_{\varepsilon_{tr}}} = \frac{8\pi}{3} g(\varepsilon_{tr}) k_BT. \tag{8}$$

Inserting Eq. (8) in Eq. (7), and using $g(\varepsilon) = N/\sqrt{2\pi\sigma^2}\exp(-\varepsilon^2/2\sigma^2)$, we get the following expression for the demarcation level:

$$\varepsilon_m(t) = \varepsilon_{tr}\left(1 + \frac{\varepsilon_{tr}}{\sigma^2/k_BT}\right) - k_BT \ln\left[\left(N_F\frac{k_BT}{\sigma}\right)^2 \frac{2}{\theta\pi}\frac{t}{\tau}\right], \tag{9}$$

where $N_F = (4\pi/3)R_F^3 N$.

According to Eq. (9), in the course of time, the demarcation level sinks to deeper energies. However, we note that this can continue only until time $t = \tau$, which is the intrinsic lifetime of the exciton. If we interpret the demarcation energy as a quasi-Fermi level [54], at time τ most excitons are accumulated around an energy level at which the product $g(\varepsilon)f[\varepsilon, \varepsilon_m(\tau)]$ maximizes. This energy is in fact the same energy ε_τ shown in Fig. 1. ε_τ is in general different from ε_∞, but if the thermalization is completed during the exciton lifetime, we obtain $\varepsilon_\tau = \varepsilon_\infty$. The energy, ε_τ is experimentally available through fluorescence spectroscopy. We stress that our model can also be applied for exciton transport in the presence of quenching centers [21,55]. In such a situation, one has to consider the demarcation energy at time $t < \tau$.

The five energy levels discussed here, ε_{tr} (TE level), ε_τ (energy relaxation during exciton lifetime), $\varepsilon_m(\tau)$ (demarcation or quasi-Fermi level at time $t = \tau$), ε_∞ (thermal equilibrium energy), and ε_F (equilibrium Fermi level), are plotted in Fig. 3 for $R_F = 5$ nm. We have used $\theta \approx 0.2$ since it gives excellent agreement with kinetic Monte Carlo (kMC) simulations, see below. As expected, at high disorder normalized temperatures the thermalization is nearly complete, and therefore ε_τ coincides with ε_∞. However, by decreasing k_BT/σ, ε_τ deviates from ε_∞, owing to the incomplete thermalization during the exciton lifetime.

Two temperature regions in Fig. 3 need to be discussed in detail. (i) Region with $\varepsilon_m(\tau) > \varepsilon_\infty$. The relaxation energy ε_τ in this region reaches a minimum at a critical temperature where $\varepsilon_m(\tau) \approx \varepsilon_\infty$, and then *increases* by decreasing the temperature, see inset of Fig. 3. This behavior, usually assigned to frustrated relaxation, has been observed experimentally [30,31], and has been predicted through kMC simulations to occur also for Förster energy transfer [38]. Here, we see that our model can naturally produce the frustrated relaxation feature, see Sec. III D for more details. (ii) Region with $\varepsilon_m(\tau) > \varepsilon_{tr}$. In the

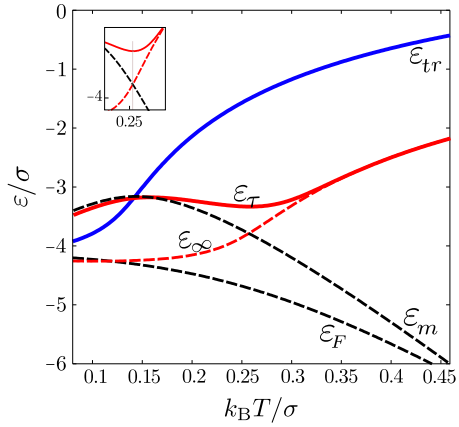

FIG. 3. ε_{tr} (TE level), ε_τ (energy relaxation during the exciton lifetime), $\varepsilon_m(\tau)$ (quasi-Fermi level), ε_∞ (thermal equilibrium energy), and ε_F (equilibrium Fermi level), as a function of disorder normalized temperature. Data are calculated using Eqs. (5) and (9) for $R_F = 5$ nm.

temperature region given by the above condition, the multiple-trapping model is not applicable at all and introducing $\varepsilon_m(\tau)$ is physically meaningless. In this region, excitons created in the system move, on average, downward toward the TE energy level, and therefore the picture of activation to a TE level is not correct. As we discuss below in the kMC section, an agreement between theory and simulation is not expected in this temperature region.

An important feature of the Förster-type transport mechanism is that the exciton transfer rate is coupled to the spontaneous decay rate, $1/\tau$; see Eq. (1). Therefore, a longer exciton lifetime does not result in a higher degree of the thermalization, because the transfer rate, that determines the degree of thermalization, is also reduced. As a consequence, as predicted by Eq. (9), the demarcation energy at time $t = \tau$, and hence ε_τ, are independent of the exciton lifetime. On the other hand, ε_τ is a strong function of the Förster radius. We discuss this dependency below, when presenting the kMC simulation results.

B. Exciton diffusion length

An important physical quantity related to exciton transport is the diffusion length. In what follows, we derive an expression for the exciton diffusion length using the TE level concept. Since the diffusion length is given by [56]

$$L_D = \sqrt{D\tau}, \tag{10}$$

we must first find the diffusion coefficient D. To obtain this, one can use [57]

$$D \approx R^2_{\varepsilon_{tr}}/\langle t\rangle, \tag{11}$$

where $\langle t\rangle$ is the mean time that excitons spend in an energy state before activation to the TE level. $\langle t\rangle$ can be obtained by averaging the quantity $1/\nu(\varepsilon \to \varepsilon_{tr})$ for energies smaller than ε_{tr} [57,58]:

$$\langle t\rangle = \tau\left(\frac{R_{\varepsilon_{tr}}}{R_F}\right)^6 \frac{\int_{-\infty}^{\varepsilon_{tr}} \exp\left(\frac{\varepsilon_{tr}-\varepsilon}{k_BT}\right) g(\varepsilon) f'[\varepsilon, \varepsilon_m(\tau)]\mathrm{d}\varepsilon}{\int_{-\infty}^{\varepsilon_{tr}} g(\varepsilon) f'[\varepsilon, \varepsilon_m(\tau)]\mathrm{d}\varepsilon}. \tag{12}$$

Combining Eqs. (10)–(12), as shown in Appendix B, we get the following expression for the diffusion length:

$$L_D \approx \left(\frac{9\theta^3}{16\pi^2}\frac{N'-n'}{n'^3}\right)^{1/6}, \tag{13}$$

where $n' = \int_{-\infty}^{\varepsilon_{tr}} g(\varepsilon) f[\varepsilon, \varepsilon_m(\tau)]\mathrm{d}\varepsilon$ and $N' = \int_{-\infty}^{\varepsilon_{tr}} g(\varepsilon)\mathrm{d}\varepsilon$. Note that, since according to Eq. (9) $\varepsilon_m(\tau)$ is a function of the Förster radius R_F, the diffusion length is also R_F dependent. However, it is clear from Eq. (13) that the dependency of L_D on R_F is more complex than that traditionally expected, that is, $L_D \propto \sqrt{D} \propto \sqrt{\nu} \sim R_F^3$ (which is deduced from a simple nearest neighbor random walk picture). This is because, for the problem of exciton transport in energetically disordered systems, R_F is not merely a multiplicative factor, but according to Eq. (9), it also controls the thermalization process, which, in turn, affects the dispersivity of the diffusion process. Another important result of our theory, as discussed in Appendix C, is that both the quantity ε_τ/σ and the diffusion length L_D in Eq. (13) scale with the dimensionless disorder strength σ/k_BT. Indeed, the scaling of both the exciton diffusion length and spectral relaxation has been predicted in the past by one of the authors using Monte Carlo simulations [19,39,59]. In the following section, we test the validity of our approach to the problem of nonequilibrium exciton transport against Monte Carlo simulations.

C. Kinetic Monte Carlo simulations

Monte Carlo simulations provide an insightful and predictive computational method for studying incoherent hopping transport phenomena in disordered semiconductors. In this paper, we use a kMC method [19] to simulate the time evolution of singlet exciton transport, confirm the validity of the developed theoretical model and test its applicability range. The computational protocol is as follows.

We consider a regular cubic cell of 40 nm × 40 nm × 40 nm with a lattice constant $a = 1$ nm. Each lattice point corresponds to an exciton transport site, while periodic boundary conditions are implemented along all directions of the cell using the minimum image criterion. Individual Monte Carlo runs start by placing one exciton at a random site in the cell with each site having an energy drawn from a Gaussian distribution with a zero mean and variance σ^2. Förster transfer rates ν_{ij} from the exciton occupied site i to each neighboring hopping site j, within a cutoff radius of $r_{cut} = 5$ nm, are calculated using Eq. (1). At each Monte Carlo step, waiting times for each hopping event are calculated according to $\tau_{ij} = -\frac{1}{\nu_{ij}} \ln X$, with X a random number from a box distribution from zero to unity, resulting in 514 events for the chosen cutoff radius. An additional waiting time for exciton recombination is computed as $\tau_{ir} = -\tau \ln X$. If the event with the shorter waiting time is a hopping event, then exciton transfers to the new site and

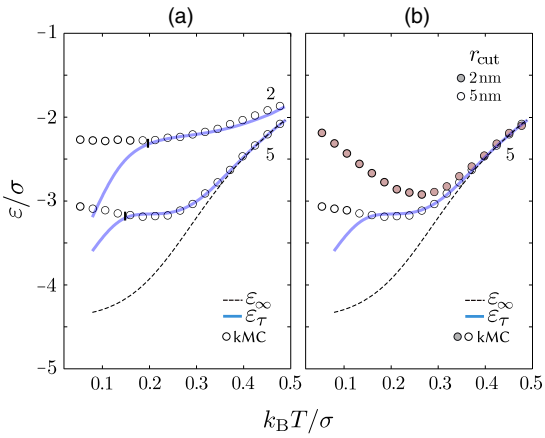

FIG. 4. (a) Energy relaxation during the exciton lifetime, ε_τ as a function of disorder normalized temperature. kMC simulations (circles) and theory (solid lines), for two different Förster radii, $R_F = 2$ and 5 nm. The critical points at which $\varepsilon_m(\tau) = \varepsilon_{tr}$, are indicated as segments. Dashed line indicates the thermal equilibrium energy ε_∞. (b) Same as (a) with $r_{cut} = 5$ nm (empty circles) and 2 nm (filled circles).

simulation advances whereas if it is recombination, the exciton is removed from the system and the run is terminated. By averaging over 10^5 individual exciton trajectories, we obtain the quantities of interest, i.e., the relaxation energy ε_τ and the diffusion length L_D. The first is calculated from the final energy of each exciton before recombination, while the latter from the displacement between the initial, exciton generation, and the final, exciton recombination, position. We allow to vary independently the temperature T and Förster radius R_F parameters, while disorder σ and lifetime τ remain constant. In fact, due to the Förster rate inverse dependence on τ, τ does not impact neither the ε_τ nor the L_D values, while a scaling law exists for both of them with respect to the dimensionless disorder parameter σ/k_BT [19,38].

The central results comparing theory with Monte Carlo simulations are presented in Fig. 4 for the spectral relaxation and Fig. 5 for the diffusion length. Figure 4(a) shows the Monte Carlo results for ε_τ, for two Förster radii $R_F = 2$ and 5 nm. The theoretical predictions, calculated based on the TE concept and using the averaging method (see Appendix D), are also shown in the figure. As pointed out above in Fig. 4(a), the multiple-trapping picture is not valid when $\varepsilon_m(\tau) > \varepsilon_{tr}$. The exact points at which $\varepsilon_m(\tau) = \varepsilon_{tr}$ are calculated and marked in the figure. In the region where the TE concept is applicable, the theory is in very good agreement with the kMC results. Since the density of the energy levels is higher near the center of the Gaussian distribution, most excitons generated in the system will have energies $\varepsilon \approx 0$ and according to the TE concept, those excitons initially move, *on average*, downward to the TE level ε_{tr}. However, en route to the TE level, some upward in energy jumps are also necessary to avoid the blockade of excitons due to disorder. Therefore, for larger Förster radii, the TE concept is valid over a broader range of temperatures, because a larger R_F results to a higher probability to overcome local energy barriers.

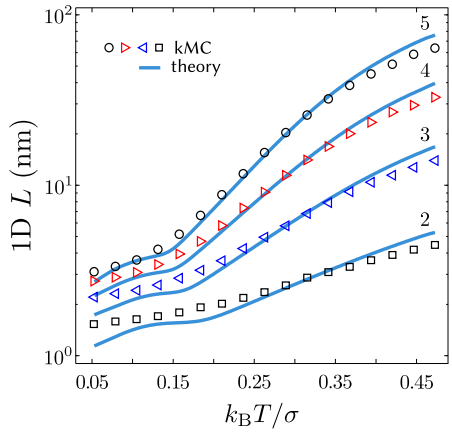

FIG. 5. Diffusion length L_D as a function of disorder normalized temperature. Data from kMC simulation (symbols) and theory (solid lines), for different Förster radii, $R_F = 2,\ 3,\ 4$, and 5 nm.

A recent combined experimental and computational study highlighted the dominant contribution of long-distance jumps to singlet exciton migration in metal-organic frameworks [60]. To illustrate the importance of long-distance hopping, we have also performed simulations with $r_{cut} = 2$ nm (i.e., restricting exciton hopping only to the first 32 nearest neighbors). Figure 4(b) shows that in comparison to $r_{cut} = 5$ nm (514 nearest neighbors), the energy relaxation shows a pronounced frustrated dynamics, inconsistent with the theory prediction. This clearly demonstrates that especially at low temperatures, long-range jumps contribute significantly to the relaxation process. In other words, due to the long-range nature of the Förster mechanism, modeling the singlet exciton transport as a simple nearest-neighbor random walk process may result in an incorrect description of the energy transfer dynamics. We can also conclude that for inherently short-range transport mechanism, like charge or triplet exciton transport problem, a strong frustration is expected, as indeed reported in earlier simulations [38,39]. We revisit this issue in more detail in Sec. III D, below.

Figure 5 compares L_D obtained from the kMC simulations with those calculated using Eq. (13). Apart from an additional constant factor (≈ 1.5) needed to fit the theory to the simulation (see Sec. III E), the theoretical results are in good agreement with the kMC simulations showing a steep increase of the diffusion length with disorder normalized thermal energy. We point out that in contrast to spectral relaxation, reliable estimates for L_D from the theoretical model can be obtained even in the regime where $\varepsilon_m(\tau) > \varepsilon_{tr}$ as L_D is less sensitive to $\varepsilon_m(\tau)$ in that region. It must be noted that our results are in agreement with experimental reports on the temperature dependence of the exciton diffusion length [29,32]. Finally, Fig. 6 shows that the traditional picture of $L_D \propto R_F^3$ does not hold true at the intermediate and low temperature region, as predicted and discussed in the theory section above.

D. TE level for short vs long-range transfer and comparison with experiment

Herein, we discuss the main differences on the TE level for short vs long-range excitation transfer and the resulting influence on energy relaxation. We also include a comparison

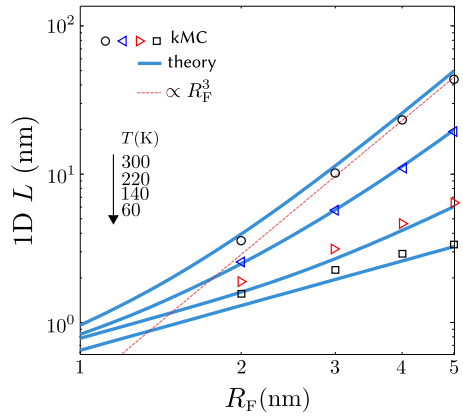

FIG. 6. Diffusion length L_D as a function of the Förster radius for different temperatures on a log-log scale. Data from kMC simulations (symbols) and theory (solid lines). Dashed line indicates the slope expected from $L_D \propto R_F^3$.

with published experimental data of temperature dependent fluorescence relaxation in organic semiconductors. Although in this paper we have focused on the hopping dynamics of singlet excitons that transfer by a Förster process, i.e., with a long-range transfer rate that is $\propto \tau^{-1}(R_F/R)^6$, within a Gaussian DOS, of particular interest is also the relaxation process of charge carriers and triplet excitons that follow a Dexter type of transfer mechanism. This short-range transfer process requires wave-function overlap and can be described by a Miller-Abrahams (MA) type of rate $\propto \nu_0 \exp(-2R/\alpha)$. An important difference between those two transfer mechanisms is that whilst for Förster transfer, exciton transport and decay are coupled to each other, due to the inverse dependence of the rate on the exciton lifetime τ, for MA transfer the attempt to hop frequency prefactor ν_0 is independent of the lifetime, with typically $\tau \gg \nu_0^{-1}$.

The TE level has been used before to study energy relaxation of charges and triplet excitons that transfer by short-range hopping rate transfer [34,53,61]. Motivated by experimental observations of photoluminescence spectra [30,31] that show a nonmonotonic dependence of the relaxation energy upon cooling, those studies along with kMC simulations [34,38,39] have revealed that charges and triplet excitons show a strong frustrated relaxation, of the order of a few σ, as depicted schematically in Fig. 7(a). To describe this behavior, we first note that the TE level for short-range transfer (MA rate) [47,62] lies above the TE level for Förster transfer across the intermediate and low temperature range, as shown in Fig. 7(b). We highlight that for MA transfer, ε_{tr} is a function of disorder normalized thermal energy k_BT/σ, exciton density N, and localization length α and is independent of ν_0. For Förster transfer, however, ε_{tr} is only a function of k_BT/σ and is independent of N, R_F, and τ. The relative position of the pertinent TE levels is therefore valid for any combination of transport parameters, unless for very large, unrealistic values of α. According to the multiple-trapping picture, upward excitation hops are mainly at the vicinity of the TE level. Henceforth, for short-range MA transfer, with decreasing thermal energy such

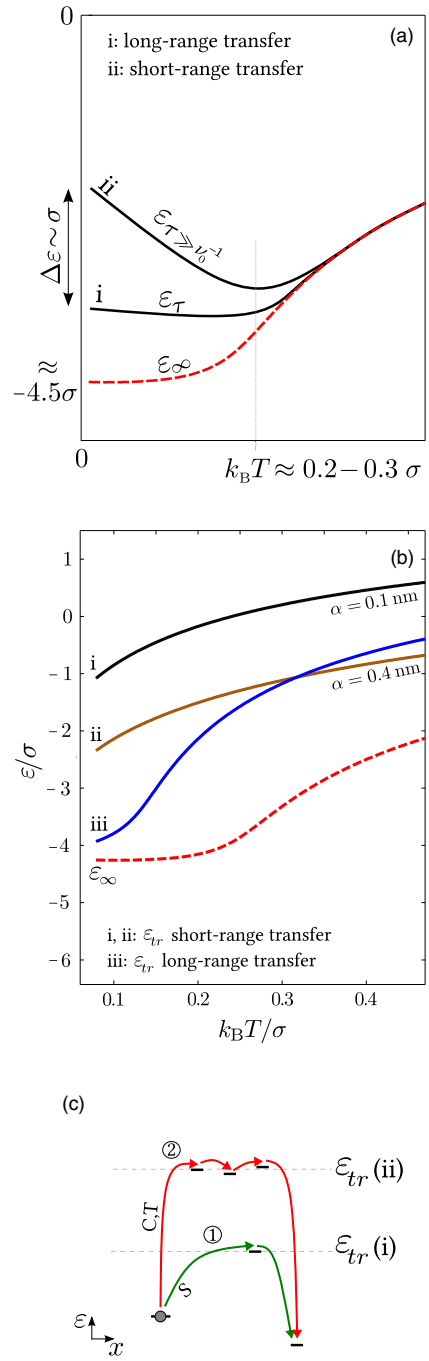

FIG. 7. (a) Illustration of temperature-dependent energy relaxation for long- vs short-range transfer processes. Short-range transfer (relevant for charges and triplet excitons) results in a strong frustration, of the order of σ at low temperatures. (b) Relevant ordering of temperature-dependent TE levels for long-range (Förster rate) and short-range (MA rate) transfer for typical transport parameters. (c) Schematic illustration showing the different relaxation pathways for charges and triplet excitons (C,T) and singlet excitons (S). The TE level for long-range transfer, i, lies below the TE level for short-range transfer, ii. Paths ① and ② result to relaxation toward deep energy levels. At intermediate and low temperatures, however, thermal activation via path ② is forbidden, leading to frustrated relaxation.

hops are less probable and the relaxation process terminates at higher energies, because intermediate activations to the TE level are necessary to reach the equilibrium level. This is schematically shown in Fig. 7(c). On the other hand, since the TE level for long-range Förster transfer is at lower energies, thermal activations to this level are more likely and therefore subsequent relaxation to deep energy levels is an allowed process. Note that although for a Gaussian DOS, sites with low energy levels are limited, the long-range nature of the Förster rate makes upward energy jumps more probable for singlet excitons [Path ① in Fig. 7(c)]. It is well established that for disordered organic semiconductors and colloidal quantum dots, a Gaussian DOS describes the distribution of localized energy states [18], whereas for inorganic semiconductors an exponential DOS is a more appropriate choice [34,61,63,64]. An important feature of the Gaussian DOS, in contrast to the exponential one, is that for a broad temperature range the most populated energy level (ε_∞ or ε_τ) does not lie near the Fermi level (ε_F or ε_m); see Fig. 3. Therefore, for calculating the amount of the energy relaxation, we have used the energy ε_τ and not the demarcation energy ε_m. For an exponential DOS however, since $\varepsilon_{\infty(\tau)} \simeq \varepsilon_{F(m)}$, one can use the position of the demarcation energy as the energy relaxation, as done in Refs. [34,61] for short-range type of transfer in an exponential DOS.

Finally, we compare our theoretical results for the energy relaxation (ε_τ) based on the TE level formulation with previously published experimental data in conjugated polymers and oligomers. Figure 8 shows experimental data obtained from the fluorescence spectra of four different films: dioctyloxy-poly(*p*-phenylene) (DOOPPP), polyfluorene (PF2/6), ladder-type poly(*p*-phenylene) (MeLPPP), and PF2/6 trimer (Trimer) as reported in Refs. [30,38]. It is evident that the theory reproduces the experimental data for reasonable Förster radii (best fits are obtained with $R_F = 2.5$ and 4.5 nm, as indicated in the figure). Note that according to Eq. (9), the quantity $N R_F^3$ is the fit parameter. Here, however, we have decided to fix the total density of states ($N = 1\ \mathrm{nm}^{-3}$) and only vary the Förster radius to obtain the above data. In Fig. 8, in addition to ε_τ, we also display ε_∞ (energy relaxation at equilibrium) and the quantity $-\sigma^2/k_BT$. Interestingly, the equilibrium quantity ε_∞ fits the experimental data for the DOOPPP polymer over the whole temperature range, showing that singlet excitons reach equilibrium conditions during their lifetime. This, in turn, is a result of the high density of localized states, a large Förster radius, or a combination of these two factors.

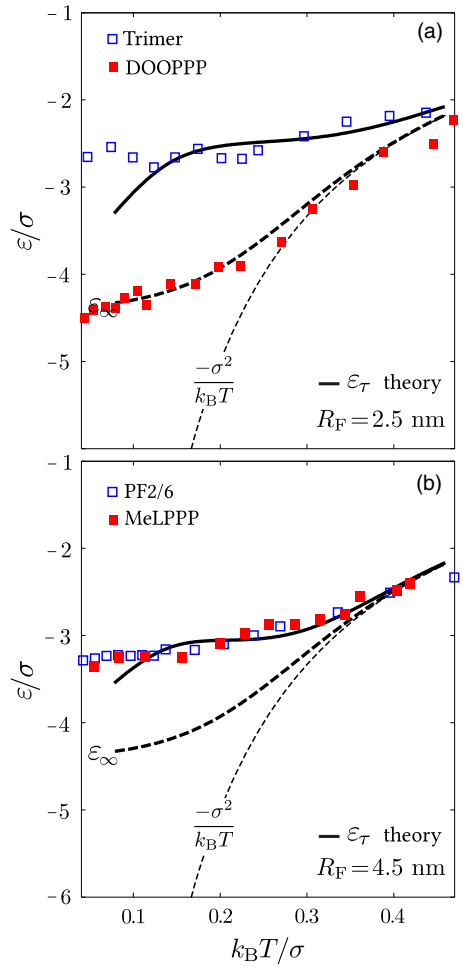

FIG. 8. Energy relaxation during the exciton lifetime, ε_τ as a function of disorder normalized temperature. Theoretical data based on the TE level (solid line) and experimental data obtained from the fluorescence spectra of (a) PF2/6 trimer (empty squares) and DOOPPP polymer(filled squares) films (from Ref. [30]) and (b) PF2/6 (empty squares) and MeLPPP (filled squares) polymer films (from Ref. [38]). The Förster radii R_F used in the calculations are indicated in the plots. The levels ε_∞ (thick dashed line) and $-\sigma^2/k_BT$ (thin dashed line) are also plotted.

E. Subdiffusive transport

Having established the effectiveness of the analytical model to describe spectral relaxation, we now turn our attention to obtaining the time dynamics of exciton diffusion. Very recently, it has been reported experimentally that exciton diffusion in a system of disordered colloidal quantum dots is dispersive and can be described as a subdiffusive transport [3], in which $D(t) \propto t^\beta$ with $\beta < 0$. Similar results have been obtained from Monte Carlo simulations for triplet exciton and charge transport in a Gaussian DOS [39,65]. To investigate whether our model can explain these observations, we expand the TE concept to take into account the time dependence of the dynamics for $t < \tau$. This can be achieved by considering the demarcation energy $\varepsilon_m(t)$, instead of $\varepsilon_m(\tau)$ used in the previous calculations. Below, we present results for the energy relaxation shift $\varepsilon_{t\leqslant\tau}$ and the diffusion coefficient $D(t)$, while we derive the time-dependent expressions in Appendix B.

Figure 9 shows the temporal evolution of $\varepsilon_{t\leqslant\tau}$ and $D(t)$ for two different temperatures and two Förster radii, $R_F = 2$ and 5 nm. As seen in Fig. 9(a), in the course of time, excitons relax to lower energy levels. For a Förster radius of $R_F = 5$ nm and at high temperatures, excitons reach the equilibrium energy during their lifetime [this is also apparent in Fig. 4(a)] and a stationary state is indeed established at $t < \tau$. In contrast, at low temperatures and/or small Förster radius, the relaxation process is incomplete and the stationary state can not obtained. Interestingly, our theoretical results for low temperatures show a linear dependence with time in the logarithmic scale $\varepsilon_{t\leqslant\tau} \sim -\ln(t/\tau)$, with the same slope for both $R_F = 2$ and

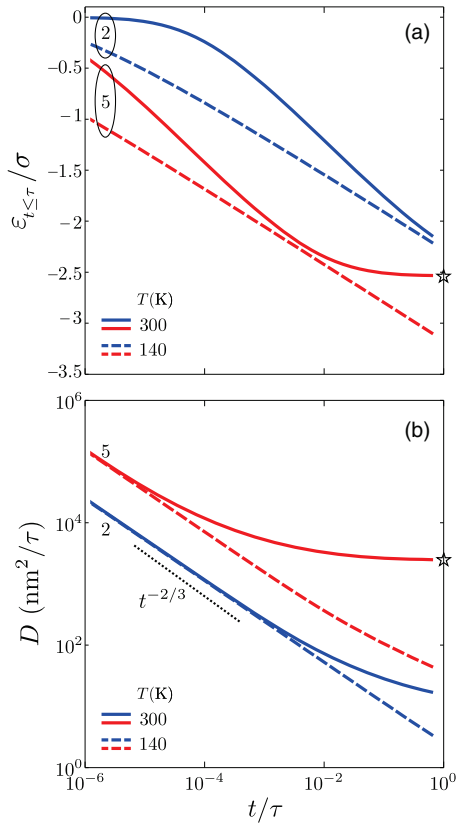

FIG. 9. (a) Energy relaxation (shift) as a function of time. Data for $T = 140$, and 300 K, and $R_F = 2$ and 5 nm. (b) Diffusion coefficient $D(t)$ as a function of time calculated using Eq. (B5). Data for $T = 140$ and 300 K and $R_F = 2$ and 5 nm. The dotted line shows the scaling of the diffusion coefficient with time in the nonequilibrium regime. Stars indicate the equilibrium values.

5 nm, and are in agreement with results from Movaghar *et. al.* [51]. The time evolution of the diffusivity is shown in Fig. 9(b). As a result of exciton relaxation to lower energy levels with time, based on the multiple-trapping picture, the waiting time needed to jump to the TE level increases with time. Therefore, the diffusion coefficient becomes time-dependent, i.e., dispersive transport, and decreases with time. As derived in Appendix B, in this nonequilibrium regime we obtain

$$D(t) \propto \left(\frac{t}{\tau}\right)^{-2/3}, \tag{14}$$

which clearly demonstrates the dispersive nature of singlet exciton diffusion. Nevertheless, at high temperatures and large Förster radius, since equilibrium can be established during the exciton lifetime, the diffusion coefficient approaches its equilibrium, time-independent, value.

In obtaining Eq. (13) for the diffusion length, the diffusion coefficient at time $t = \tau$ has been used in the calculations. However, since the exciton transport occurs almost entirely in the nonequilibrium regime and the diffusion coefficient is time-dependent, using $D(t = \tau)$ may result in an underestimation of the diffusion length. This argument shows why an additional factor was required to fit the theory with the kMC results in Fig. 5. One can estimate this factor by using the following relation for the diffusion length of excitons :

$$L_D = \sqrt{\int_0^\tau D(t)\mathrm{d}t}. \tag{15}$$

Using Eq. (14) we have

$$L_D \approx \sqrt{D(\tau)\tau \int_0^\tau (t/\tau)^{-2/3}\mathrm{d}(t/\tau)} = \sqrt{3} \times \sqrt{D(\tau)\tau}. \tag{16}$$

The factor $\sqrt{3}$ justifies the additional factor used in Fig. 5 to match the theory with the kMC results.

IV. CONCLUSION

A theory for singlet exciton hopping transport has been developed and tested. It describes diffusive transport via long-range Förster transfer in a Gaussian distribution of localized states through a multiple-trapping mechanism, with the TE playing the role of the mobility edge. The theory provided in this paper fully describes the transition from equilibrium to nonequilibrium transport. The global validity range of the theory is illustrated by comparison to Monte Carlo simulations. We find that for Förster radius values smaller than 5 nm, typical in organic semiconductors, exciton transport occurs mainly in the nonequilibrium regime and the diffusion length deviates from the cubic dependence upon the Förster radius. An important feature of the theory is that it takes into account explicitly the temporal evolution of the spectral relaxation energy and diffusivity and can be used to understand time-gated spectroscopic experiments in a wide range of disordered semiconducting materials. Understanding the exciton dynamics is also important for exploiting novel device applications. In the current paper, we take a step toward this goal and anticipate that it will motivate further studies. In future work, we hope to tackle the excitation density dependence of the relaxation dynamics and transport in spatially correlated disordered systems.

ACKNOWLEDGMENTS

This project has received funding from the Universidad Carlos III de Madrid, the European Union's Seventh Framework Programme for research, technological development, and demonstration under Grant Agreement No. 600371, el Ministerio de Economía, Industria y Competitividad (COFUND2014-51509), el Ministerio de Educación, cultura y Deporte (CEI-15-17), and Banco Santander.

APPENDIX A: POSITION OF THE TRANSPORT ENERGY

According to Eq. (1), the upward exciton jump rate is given by

$$\nu(\varepsilon_d \to \varepsilon_a) = \frac{1}{\tau}\left(\frac{R_F}{R}\right)^6 \exp\left(-\frac{\varepsilon_a - \varepsilon_d}{k_B T}\right), \tag{A1}$$

where $\varepsilon_a - \varepsilon_d > 0$ is the difference between the acceptor and donor energy. Let us denote this rate by $\nu_\uparrow(\varepsilon_d, \varepsilon_a, R)$. For steep energy distributions, the typical upward jump distance is given

by [Eq. (4) in the main text]

$$R_{\varepsilon_a} = \left[\frac{4\pi}{3}\int_{-\infty}^{\varepsilon_a} g(\varepsilon) f'(\varepsilon, \varepsilon_F)\mathrm{d}\varepsilon\right]^{-1/3}. \tag{A2}$$

Now, according to the standard approach of calculating the TE level, we seek to find if such an acceptor energy level exists that it maximizes all typical upward jumps, independent of the donor energy. In other words, we look for a unique acceptor energy, ε_{tr}, that meets the condition

$$\left.\frac{\partial \nu_\uparrow(\varepsilon_d, \varepsilon_a, R_{\varepsilon_a})}{\partial \varepsilon_a}\right|_{\varepsilon_a=\varepsilon_{tr}} = 0. \tag{A3}$$

By algebraic manipulation of the above equation, we obtain Eq. (5).

APPENDIX B: DIFFUSION COEFFICIENT

In this appendix, a general expression for the diffusion coefficient is obtained, from which the time-dependency of the diffusion coefficient and the singlet diffusion length can be extracted. First, we note that the integral in the numerator of Eq. (12) can be rewritten as

$$\exp\left(\frac{\varepsilon_{tr}-\varepsilon_m}{k_\mathrm{B}T}\right)\int_{-\infty}^{\varepsilon_{tr}} \exp\left(\frac{\varepsilon_m-\varepsilon}{k_\mathrm{B}T}\right) g(\varepsilon) f'(\varepsilon, \varepsilon_m)\mathrm{d}\varepsilon, \tag{B1}$$

where, for brevity, we have used ε_m for $\varepsilon_m(t)$. This, bearing in mind that $f' = 1 - f$, can be simplified as

$$\exp\left(\frac{\varepsilon_{tr}-\varepsilon_m}{k_\mathrm{B}T}\right)\int_{-\infty}^{\varepsilon_{tr}} g(\varepsilon) f(\varepsilon, \varepsilon_m)\mathrm{d}\varepsilon. \tag{B2}$$

On the other hand, using Eq. (6), for the exponential term in the above equation we have

$$\exp\left(\frac{\varepsilon_{tr}-\varepsilon_m}{k_\mathrm{B}T}\right) = \frac{t}{\tau\theta}\left(\frac{R_\mathrm{F}}{R_{\varepsilon_{tr}}}\right)^6. \tag{B3}$$

Using these simplifications, and if we define $n' = \int_{-\infty}^{\varepsilon_{tr}} g(\varepsilon) f(\varepsilon, \varepsilon_m)\mathrm{d}\varepsilon$ and $N' = \int_{-\infty}^{\varepsilon_{tr}} g(\varepsilon)\mathrm{d}\varepsilon$, we obtain

$$D(t) = \frac{\theta}{t} R_{\varepsilon_{tr}}^2 \frac{N'-n'}{n'}, \tag{B4}$$

that, using Eq. (4), can be rewritten as

$$D(t) = \frac{\theta}{t}\left(\frac{4\pi}{3}\right)^{-2/3}\frac{\left(N'-n'\right)^{1/3}}{n'}. \tag{B5}$$

From this general result, one can obtain Eq. (13) for the diffusion length $L_D = \sqrt{D(\tau)\tau}$.

To obtain the time-evolution of the diffusion coefficient in nonequilibrium regime, we use the fact that the demarcation energy is high at short and intermediate times such that we can write $f \approx 1$ and $1 - f \approx \exp\{[\varepsilon - \varepsilon_m(t)]/k_\mathrm{B}T\}$. Therefore, since $\varepsilon_m(t) = \varepsilon_m(\tau) - k_\mathrm{B}T\ln(t/\tau)$, we can obtain the following time-dependent behavior for the diffusion coefficient (valid only for the nonequilibrium regime):

$$D(t) \propto (t/\tau)^{-2/3}. \tag{B6}$$

On the other hand, at the equilibrium regime where the demarcation energy lies deep in the energy distribution, we can use the approximation $f \approx \exp\{-[\varepsilon - \varepsilon_m(t)]/k_\mathrm{B}T\}$ and $N' - n' \approx N'$. These approximations result in a stationary diffusion coefficient as

$$D_\mathrm{st} \propto (t/\tau)^0. \tag{B7}$$

APPENDIX C: SCALING BEHAVIOR OF THE DIFFUSION LENGTH

Equation (3) shows that at a given density n, the Fermi level ε_F is determined by the temperature and the width of the energy distribution. By expressing this integral in terms of a new variable $x = \varepsilon/\sigma$, we find that the temperature-normalized Fermi level, that is, $\varepsilon_F/k_\mathrm{B}T$, is a function of the dimensionless disorder parameter $\sigma/k_\mathrm{B}T$. Using this result, and the same change-of-variable for the integral of Eq. (5), we find that ε_{tr}/σ is a function of $\sigma/k_\mathrm{B}T$. Inspection of Eq. (9) for the demarcation level shows that the same scaling behavior holds for $\varepsilon_m(\tau)/\sigma$, and since ε_τ is the energy at which the product $g(\varepsilon) f[\varepsilon, \varepsilon_m(\tau)]$ maximizes, we find that ε_τ/σ also scales with $\sigma/k_\mathrm{B}T$. Using the above scaling features and Eq. (13), we obtain that $L_D = L_D(\sigma/k_\mathrm{B}T)$.

APPENDIX D: AVERAGING METHOD FOR THE CALCULATION OF THE RELAXATION ENERGY

The equilibrium energy ε_∞ can be calculated in two different ways. As pointed out in the main text, we have introduced ε_∞ as the energy that maximizes the product $g(\varepsilon) f(\varepsilon, \varepsilon_F)$. Accordingly, the relaxation energy ε_τ can be found by maximizing the product $g(\varepsilon) f[\varepsilon, \varepsilon_m(\tau)]$. On the other hand, one can define the equilibrium or relaxation energy as the average energy of the carriers. In this definition, the equilibrium energy is calculated as

$$\langle\varepsilon\rangle = \frac{\int \varepsilon g(\varepsilon) f(\varepsilon, \varepsilon_F)\mathrm{d}\varepsilon}{\int g(\varepsilon) f(\varepsilon, \varepsilon_F)\mathrm{d}\varepsilon}. \tag{D1}$$

To obtain ε_τ, one needs to replace ε_F with $\varepsilon_m(\tau)$ in the above equation. We find that the averaging method gives excellent agreement with Monte Carlo simulations. In comparison, the method of maximizing the product $f \times g$ results in slightly lower values for the equilibrium energy at intermediate and higher temperatures and a more pronounced minimum (Fig. 3). However, since the product $f \times g$ is approximately a symmetric function of energy, the two definitions result in the same overall trend and similar values for the relaxation energy. From a practical point of view, while the first method is numerically more tractable, the second definition is most suitable for comparing with kMC simulation results, where the relaxation energy is obtained by averaging over different exciton trajectories. Throughout this paper, we adopted the first method, except in Figs. 4 and 8 where we compare ε_τ with kMC calculations and experimental results.

[1] C. J. Bardeen, Annu. Rev. Phys. Chem. **65**, 127 (2014).
[2] O. V. Mikhnenko, P. W. Blom, and T.-Q. Nguyen, Energy Environ. Sci. **8**, 1867 (2015).
[3] G. M. Akselrod, F. Prins, L. V. Poulikakos, E. M. Lee, M. C. Weidman, A. J. Mork, A. P. Willard, V. Bulović, and W. A. Tisdale, Nano Lett. **14**, 3556 (2014).
[4] K. F. Chou and A. M. Dennis, Sensors **15**, 13288 (2015).
[5] C. Curutchet, A. Franceschetti, A. Zunger, and G. D. Scholes, J. Phys. Chem. C **112**, 13336 (2008).
[6] D. Geißler and N. Hildebrandt, Anal. Bioanal. Chem. **408**, 4475 (2016).
[7] J. Lefebvre and P. Finnie, J. Phys. Chem. C **113**, 7536 (2009).
[8] A. Ishii, M. Yoshida, and Y. K. Kato, Phys. Rev. B **91**, 125427 (2015).
[9] B. A. Ruzicka, R. Wang, J. Lohrman, S. Ren, and H. Zhao, Phys. Rev. B **86**, 205417 (2012).
[10] D. Schilling, C. Mann, P. Kunkel, F. Schöppler, and T. Hertel, J. Phys. Chem. C **119**, 24116 (2015).
[11] V. Sundström, T. Pullerits, and R. van Grondelle, J. Phys. Chem. B **103**, 2327 (1999).
[12] G. J. Hedley, A. Ruseckas, and I. D. W. Samuel, Chem. Rev. **117**, 796 (2017).
[13] J. Hou, O. Inganäs, R. H. Friend, and F. Gao, Nat. Mater. **17**, 119 (2018).
[14] F. Zhao and D. Ma, Mater. Chem. Front. **1**, 1933 (2017).
[15] C. Liu, Z. Li, T. J. Hajagos, D. Kishpaugh, D. Y. Chen, and Q. Pei, ACS Nano **11**, 6422 (2017).
[16] X. Ma, O. Roslyak, J. G. Duque, X. Pang, S. K. Doorn, A. Piryatinski, D. H. Dunlap, and H. Htoon, Phys. Rev. Lett. **115**, 017401 (2015).
[17] V. May and O. Kühn, *Charge and Energy Transfer Dynamics in Molecular Systems* (John Wiley & Sons, Weinheim, Germany, 2008).
[18] A. Köhler and H. Bässler, *Electronic Processes in Organic Semiconductors: An Introduction* (John Wiley & Sons, Weinheim, Germany, 2015).
[19] S. Athanasopoulos, E. V. Emelianova, A. B. Walker, and D. Beljonne, Phys. Rev. B **80**, 195209 (2009).
[20] R. Kersting, U. Lemmer, R. F. Mahrt, K. Leo, H. Kurz, H. Bässler, and E. O. Göbel, Phys. Rev. Lett. **70**, 3820 (1993).
[21] S. Athanasopoulos, E. Hennebicq, D. Beljonne, and A. B. Walker, J. Phys. Chem. C **112**, 11532 (2008).
[22] I. Rörich, O. V. Mikhnenko, D. Gehrig, P. W. M. Blom, and N. I. Crăciun, J. Phys. Chem. B **121**, 1405 (2017).
[23] S. M. Menke and R. J. Holmes, Energy Environ. Sci. **7**, 499 (2014).
[24] J. D. A. Lin, O. V. Mikhnenko, J. Chen, Z. Masri, A. Ruseckas, A. Mikhailovsky, R. P. Raab, J. Liu, P. W. M. Blom, M. A. Loi, C. J. Garcia-Cervera, I. D. W. Samuel, and T.-Q. Nguyen, Mater. Horiz. **1**, 280 (2014).
[25] F. Fennel and S. Lochbrunner, Phys. Rev. B **85**, 094203 (2012).
[26] S. C. J. Meskers, J. Hübner, M. Oestreich, and H. Bässler, J. Phys. Chem. B **105**, 9139 (2001).
[27] L. M. Herz, C. Silva, A. C. Grimsdale, K. Müllen, and R. T. Phillips, Phys. Rev. B **70**, 165207 (2004).
[28] C. Madigan and V. Bulović, Phys. Rev. Lett. **96**, 046404 (2006).
[29] O. Mikhnenko, F. Cordella, A. Sieval, J. Hummelen, P. Blom, and M. Loi, J. Phys. Chem. B **112**, 11601 (2008).
[30] S. T. Hoffmann, H. Bässler, J.-M. Koenen, M. Forster, U. Scherf, E. Scheler, P. Strohriegl, and A. Köhler, Phys. Rev. B **81**, 115103 (2010).
[31] M. Skolnick, P. Tapster, S. Bass, A. Pitt, N. Apsley, and S. Aldred, Semicond. Sci. Technol. **1**, 29 (1986).
[32] J. D. Lin, O. V. Mikhnenko, T. S. van der Poll, G. C. Bazan, and T.-Q. Nguyen, Adv. Mater. **27**, 2528 (2015).
[33] A. D. Stein, K. A. Peterson, and M. D. Fayer, J. Chem. Phys. **92**, 5622 (1990).
[34] S. D. Baranovskii, R. Eichmann, and P. Thomas, Phys. Rev. B **58**, 13081 (1998).
[35] K. M. Gaab and C. J. Bardeen, J. Phys. Chem. A **108**, 10801 (2004).
[36] J. M. Jean, C.-K. Chan, G. Fleming, and T. G. Owens, Biophys. J. **56**, 1203 (1989).
[37] Y. Jia, J. Jean, M. Werst, C. Chan, and G. Fleming, Biophys. J. **63**, 259 (1992).
[38] S. Athanasopoulos, S. T. Hoffmann, H. Bässler, A. Köhler, and D. Beljonne, J. Phys. Chem. Lett. **4**, 1694 (2013).
[39] S. T. Hoffmann, S. Athanasopoulos, D. Beljonne, H. Bässler, and A. Köhler, J. Phys. Chem. C **116**, 16371 (2012).
[40] T. A. Papadopoulos, L. Muccioli, S. Athanasopoulos, A. B. Walker, C. Zannoni, and D. Beljonne, Chem. Sci. **2**, 1025 (2011).
[41] E. V. Emelianova, S. Athanasopoulos, R. J. Silbey, and D. Beljonne, Phys. Rev. Lett. **104**, 206405 (2010).
[42] S. Athanasopoulos, L. Alfonso Hernandez, D. Beljonne, S. Fernandez-Alberti, and S. Tretiak, J. Phys. Chem. Lett. **8**, 1688 (2017).
[43] J. A. Bjorgaard and M. E. Köse, RSC Adv. **5**, 8432 (2015).
[44] T.-S. Ahn, N. Wright, and C. J. Bardeen, Chem. Phys. Lett. **446**, 43 (2007).
[45] M. Grünewald and P. Thomas, Phys. Status Solidi B **94**, 125 (1979).
[46] S. Baranovskii, P. Thomas, and G. Adriaenssens, J. Non-Cryst. Solids **190**, 283 (1995).
[47] S. Baranovskii, T. Faber, F. Hensel, and P. Thomas, J. Phys.: Condens. Matter **9**, 2699 (1997).
[48] B. Valeur and M. N. Berberan-Santos, *Molecular Fluorescence: Principles and Applications* (John Wiley & Sons, Weinheim, Germany, 2012).
[49] S. Baranovskii, Phys. Status Solidi B **251**, 487 (2014).
[50] S. Baranovskii and T. Faber, Phys. Status Solidi B **218**, 59 (2000).
[51] B. Movaghar, M. Grünewald, B. Ries, H. Bässler, and D. Würtz, Phys. Rev. B **33**, 5545 (1986).
[52] H. Bässler, Phys. Status Solidi B **175**, 15 (1993).
[53] T. Tiedje and A. Rose, Solid State Commun. **37**, 49 (1981).
[54] J. Bisquert, Phys. Rev. E **72**, 011109 (2005).
[55] O. V. Mikhnenko, M. Kuik, J. Lin, N. van der Kaap, T. Nguyen, and P. W. M. Blom, Adv. Mater. **26**, 1912 (2013).
[56] M. Ansari-Rad, Y. Abdi, and E. Arzi, J. Appl. Phys. **112**, 074319 (2012).
[57] S. D. Baranovskii, H. Cordes, F. Hensel, and G. Leising, Phys. Rev. B **62**, 7934 (2000).
[58] J. O. Oelerich, D. Huemmer, and S. D. Baranovskii, Phys. Rev. Lett. **108**, 226403 (2012).

[59] S. Athanasopoulos, E. V. Emelianova, A. B. Walker, and D. Beljonne, Proc. SPIE **7722**, 772214 (2010).
[60] Q. Zhang, C. Zhang, L. Cao, Z. Wang, B. An, Z. Lin, R. Huang, Z. Zhang, C. Wang, and W. Lin, J. Am. Chem. Soc. **138**, 5308 (2016).
[61] J. Orenstein and M. Kastner, Solid State Commun. **40**, 85 (1981).
[62] I. Fishchuk, V. I. Arkhipov, A. Kadashchuk, P. Heremans, and H. Bässler, Phys. Rev. B **76**, 045210 (2007).
[63] O. Rubel, S. D. Baranovskii, K. Hantke, B. Kunert, W. W. Rühle, P. Thomas, K. Volz, and W. Stolz, Phys. Rev. B **73**, 233201 (2006).
[64] C. Karcher, K. Jandieri, B. Kunert, R. Fritz, M. Zimprich, K. Volz, W. Stolz, F. Gebhard, S. D. Baranovskii, and W. Heimbrodt, Phys. Rev. B **82**, 245309 (2010).
[65] G. Schnönherr, R. Eiermann, H. Bässler, and M. Silver, Chem. Phys. **52**, 287 (1980).